MORPHOLOGICAL EVOLUTION OF GALAXIES

Hugo Martel, ¹ Premana Premadi, ^{2,3} and Richard Matzner ^{2,3,4}

ABSTRACT

We simulate the growth of large-scale structure, for 3 different cosmological models, an Einstein-de Sitter model (density parameter $\Omega_0 = 1$), an open model ($\Omega_0 = 0.2$) and a flat model with nonzero cosmological constant ($\Omega_0 = 0.2$, cosmological constant $\lambda_0 = 0.8$), using a cosmological N-body code (P³M) with 64³ dark matter particles in a comoving cubic volume of present comoving size 128 Mpc. The calculations start at z=24 and end at z=0. We use the results of these simulations to generate distributions of galaxies at the present (z=0), as follows: Using a Monte-Carlo method based on the present distribution of dark matter, we located ~ 40000 galaxies in the computational volume. We then ascribe to each galaxy a morphological type based on the local number density of galaxies in order to reproduce the observed morphology-density relation. The resulting galaxy distributions are similar to the observed ones, with most ellipticals concentrated in the densest regions, and most spirals concentrated in lowdensity regions. By "tying" each galaxy to its nearest dark matter particle, we can trace the trajectory of that galaxy back in time, by simply looking at the location of that dark matter particle at earlier time-slices provided by the N-body code. This enables us to reconstruct the distribution of galaxies at high redshift, and the trajectory of each galaxy from its formation epoch to the present.

We use these galaxy distributions to investigate the problem of morphological evolution. Our goal is to determine whether the morphological type of galaxies is primarily determined by the initial conditions in which these galaxies form, or by evolutionary processes (such as mergers or tidal stripping) occurring after the galaxies have formed, and eventually altering their morphology, or a combination of both effects. Our main technique consists of comparing the environments in which galaxies are at the epoch of galaxy formation (taken to be at redshift z=3) with the environment in which the same galaxies are at the present. Making the null hypothesis that the morphological types of galaxies do not evolve, we compare the galaxies that form in low density environments but end up later in high density environment. The first group contains a larger proportion of elliptical and S0 galaxies than the second group. We assume that the

 $^{^{1}\}mathrm{Department}$ of Astronomy, University of Texas, Austin, TX 78712

²Center for Relativity, University of Texas, Austin, TX 78712

³Department of Physics, University of Texas, Austin, TX 78712

⁴Orson Anderson Scholar, Los Alamos National Laboratory 1996-97

initial galaxy formation process cannot distinguish a low density environment that will always remain low density from one that will eventually become high density. Therefore, these results are absurd and force us to discard the null hypothesis that morphological evolution does not occur. Our study suggests that $\sim 75\%$ of the elliptical and S0 galaxies observed at present formed as such, while the remaining $\sim 25\%$ of these galaxies formed as spiral galaxies, and underwent morphological evolution, for all three cosmological models considered (the percentages might be smaller for elliptical than S0 galaxies). These numbers assume a morphological evolution process which converts one spiral galaxy into either a S0 or an elliptical galaxy. If the morphological evolution process involves mergers of spiral galaxies, these numbers be would closer to 85% and 15%, respectively. We conclude that most galaxies did not undergo morphological evolution, but a non-negligible fraction did.

Subject headings: galaxies: clusters of — galaxies: evolution — galaxies: formation — galaxies: structure — large-scale structure of universe

1. INTRODUCTION

1.1. Morphological Types

Galaxies exist in several forms, elliptical, lenticulars, spirals, and irregulars, usually referred to as morphological types. Elliptical galaxies are featureless, ellipsoidal stellar systems composed of old Population II stars, with no appreciable amount of cold gas or dust. In addition, many of them are known to contain also a disk. Ellipticals galaxies are labeled as E0, E1, and so on, according to their ellipticity. Lenticular galaxies have a prominent, featureless disk, that contains no appreciable amount of cold gas or dust, and no spiral arms. They are very similar to the most elongated, E7 elliptical galaxies. These galaxies are labeled as S0. Spiral galaxies are composed of a disk of Population I stars, cold gas, and dust, arranged in a pattern of spiral arms, and a central bulge of population II stars which resemble small elliptical galaxies. The spiral arms are the site of active star formation, and contain a large number of young O and B stars. Spiral galaxies have flat rotation curves that extend to radii well beyond the visible edge of the galaxy, thus implying that these galaxies are imbedded into large dark matter halo. Spiral galaxies are labeled as Sa, Sb, Sc, and Sd galaxies according to their disk-to-bulge luminosity ratio (D/B), with the bulge dominating the luminosity for Sa galaxies, and the disk dominating for Sd galaxies. Galaxies that do not belong to any of these categories are classified as irregular galaxies. Some irregular galaxies result from collision and merging between galaxies, but the majority of irregular galaxies are small, gas rich galaxies similar to the Magellanic clouds. We label these galaxies as Im.

All the galaxy types described above can be combined into a single sequence, $E0 \rightarrow E1 \rightarrow ... \rightarrow E7 \rightarrow S0 \rightarrow Sa \rightarrow Sb \rightarrow Sc \rightarrow Sd \rightarrow Im$, called the *Hubble sequence*. Near the start of the sequence, galaxies are mostly composed of old Population II stars, with no dust and no cold gas, and therefore no active star formation, and a small disk-to-bulge ratio. As we move along the sequence, the preponderance of Population II stars decreases in favor of younger, Population I stars. The amount of dust and cold gas increases, D/B increases, and star formation becomes important.

A successful theory of galaxy formation must be able to explain the existence of the Hubble sequence, the origin of each morphological type, their relative abundance, and their clustering properties. To achieve this goal, we must first identify and understand the physical processes that are involved in the galaxy formation

process, as well as the processes that might subsequently alter the structure of galaxies after they are formed. The most important clue for understanding the galaxy formation process is the existence of a *Morphology-Density Relationship* relating the likelihood of any given galaxy to have a particular morphological type to the *local* density of the environment in which that galaxy is located.

1.2. The Morphology-Density Relation at Present

There is a significant difference between the galaxy populations of nearby low-density fields and in the densest regions inside nearby clusters of galaxies. Though all morphological types are present both in clusters and in the field, field galaxies are predominantly spirals, while clusters of galaxies contain a much larger proportion of elliptical and S0 galaxies. Furthermore, population gradients are found inside clusters. Melnick & Sargent (1977) showed that the proportion of spiral galaxies increases as a function of the distance from the cluster center, with a corresponding decrease in the proportion of S0 and elliptical galaxies. Dressler (1980) argued that this morphology-radius relation is applicable only to regular, spherical clusters with a well-defined center. Most clusters are highly irregular, and often contain several high density concentrations, or lumps. The distribution of the various morphological types inside these lumps is similar to the one in the center of the regular, spherical clusters. Dressler (1980) concluded that the correct way to describe the distribution of morphological types is in terms of the local number density of galaxies, and not the distance from the cluster center. Using a sample of 55 rich clusters, he showed that the fraction of elliptical and So galaxies increases with increasing surface number density of galaxies, with a corresponding decrease in the fraction of spiral galaxies, over 3 orders of magnitude in surface number density. The lowest density regions in the sample are composed of 80% spirals, 10% S0's, and 10% ellipticals, while the densest clumps are composed of 10% spirals, 40% So's, and 50% ellipticals. Subsequent studies (Bhavsar 1981; de Souza et al 1982; Postman & Geller 1984) confirmed the relations derived by Dressler (1980), and extended them to the low-density field. All these results are summarized in Dressler (1984). The morphology-density relation extends over 5 orders of magnitude in volume number density (Postman & Geller claim 6 orders of magnitude), and is a slowly varying, monotonic relation. The lowest-density regions are composed of 80–90% spirals, while the highest-density regions are composed of 80–90% ellipticals and So's. (Notice that a recent paper by Withmore, Gilmore, & Jones [1993] challenges the existence of the morphology-density relation, and claims that the morphology-radius relation is actually the correct one.)

1.3. The Origin of the Morphological Types

Several galaxy formation models have been suggested to explain the origin of the Hubble sequence and the existence of the morphology-density relation. Dressler (1984) has grouped these various models into three classes, based on the relative importance of initial conditions and evolution processes in determining the final morphological type of galaxies. We shall follow the same classification here.

1.3.1. Morphological Evolution

Models that belong to the first class all assume that galaxies form in similar environments, and therefore the existence of different morphological types does not result from different initial conditions, but instead from evolutionary processes happening after the galaxies have formed. Several models have been suggested to explain the abundance of S0 galaxies and deficiency of spiral galaxies in dense regions. These models all assume that S0 galaxies are spiral galaxies that have lost their gas and dust as a result of some evolutionary process taking place in the dense environments of cluster cores. The various possible physical mechanism for gas stripping include direct collisions (Spitzer & Baade 1951) ram-pressure stripping (Gunn & Gott 1972) and gas evaporation by a hot intracluster gas (Cowie & Songaila 1977). Dressler (1980) pointed out a major problem with these models: the various physical mechanisms suggested are efficient only in the densest regions, inside cluster cores. Though the fraction of S0 galaxies is largest in these regions, the actual number of S0's galaxies in these regions is small. About 80% of S0 galaxies are located in intermediate-density regions. Spiral galaxies in intermediate-density regions are deficient in gas by a factor of 2-3 relative to field spirals, indicating that gas ablation is important in these regions as well (Giovanelli, Chincarini, & Haynes 1981; Bothun, Schommer, & Sullivan 1982; Kennicutt 1983). However, this effect is much too weak to explain the presence of S0 galaxies, which are gas deficient by a factor of 100 relative to field spirals.

1.3.2. Initial Conditions Combined with Morphological Evolution.

The second class of models comprises all models in which both initial conditions and morphological evolution play an important role in determining the morphological types of galaxies. Kent (1981) had suggested that the morphology-density relation originates from the "fading" of disks in high density regions. In this model, initial conditions are assumed to be responsible for determining the initial morphological type of disk galaxies, such that disk galaxies with large D/B become predominantly spirals, while disk galaxies with small D/B become predominantly S0's. The model then assumes that the disks of spiral and S0 galaxies are fainter in high density regions than in low density region (this could result from the dissipation of the disk by tidal interaction, or, if the disks are still in the process of forming, then a large density environment might disrupt this process). The fading of disks causes some spiral galaxies to become too faint to be observable, and others to be identified as S0 galaxies. Furthermore, the fading of the disk of S0 galaxies causes some of these galaxies to be identified as ellipticals. With an appropriate choice of parameters, this model can successfully reproduce all the relations given in Dressler (1980). Larson, Tinsley, & Caldwell (1980) have proposed a similar model, based on the time scale for gas exhaustion via stellar evolution in disks. In their model, the gas exhausted by star formation is constantly replaced by gas infalling from a gaseous envelope surrounding the galaxy. In high-density regions, tidal encounters would disrupt this envelope, resulting in a progressive fading of the disk as stellar evolution proceeds. The various gas-stripping processes mentioned in §1.3.1 could be responsible for transforming spirals galaxies into S0's inside cluster cores (even though they cannot account for the existence of field S0 galaxies). Byrd & Valtonen (1990) have argued that the interaction of spiral galaxies with the tidal field of the cluster is a more efficient process than ram pressure stripping in depleting these galaxies of their interstellar gas, and eventually turning them into S0 galaxies (but not ellipticals). Their model is supported by the abundance of barred spiral galaxies in the core of the Coma cluster, since the formation of a bar in a normal spiral galaxy can also result from strong tidal interaction.

If the galactic disks are "faded" in high density regions, as these models assume, then the luminosity function inside dense clusters should differ significantly from the one in low density clusters and in the field. However, observations show that the luminosity functions in low- and high-density regions are essentially identical (Dressler 1984, and references therein), though Biviano et al. (1995) recently suggested that this might not be the case for the Coma cluster. In order to maintain the luminosity function unchanged in high-density regions, any "fading" of the disk must then be accompanied by a corresponding brightening of the

bulge. Mergers could be responsible for building up large galactic bulges in high-density regions. It has been suggested that elliptical galaxies result from the merging of spiral galaxies (Toomre & Toomre 1972; Toomre 1977; White 1978; 1979; Fall 1979). Ross (1981) has suggested that galaxies form mainly as stellar disks, and that galactic bulges are formed by merging, for all galaxy types. This could explain the fact that the angular momenta of disk and bulge in disk galaxies are almost perfectly aligned (Gerhard 1981). Numerical simulations of galaxy mergers by Mihos & Hernquist (1994a, 1994b) support this model, by showing that mergers trigger infall of material toward the center of the system. This model, if correct, would explain the abundance of both S0 and elliptical galaxies in high-density regions. Numerical simulations (Efstathiou & Jones 1979; Aarseth & Fall 1980) have shown that mergers of galaxies on highly eccentric orbits result in the slow-rotating systems, consistent with measurements of the spin parameter for elliptical galaxies.

Merging events, however, are not expected to occur inside rich clusters, where most ellipticals are found. The velocity dispersion in these regions is quite high, resulting in a significant reduction of the gravitational cross sections of galaxies. More likely, mergers occur inside small groups of galaxies where the velocity dispersion is smaller, and later these groups assemble into clusters (see, e.g., Geller & Beers 1982). Numerical simulations (Aarseth & Fall 1980; Negroponte & White 1983; Noguchi 1988; Barnes 1989; Barnes & Hernquist 1991; 1992) show that galaxy mergers occur naturally inside small groups, and that such mergers result in the formation of spheroidal galaxies with essentially no disk (Barnes & Hernquist 1992). Baugh, Cole, & Frenk (1996) have used a semi-analytical, Monte Carlo model to describe galaxy mergers in a standard Cold Dark Matter (CDM) universe. Their model produces a distribution of D/B which are consistent with observations, when the values of D/B are used to ascribe morphological types. Moore et al. (1996) have suggested that morphological evolution of spirals actually occurs inside dense clusters, in spite of the large velocity dispersion. In their model, called "galaxy harassment," spiral galaxies are disrupted by the cumulative effect of several high velocity close encounters with other galaxies.

The various studies of mergers described above consider the merging of two or more galaxies of comparable size. A completely separate problem is the merging of a disk galaxy with a satellite galaxy of much smaller mass. These merging events can modify the structure of the disk, but the effect is too small to result in actual morphological evolution (that is, spiral galaxies will remain spiral after "swallowing" a satellite). Numerical simulations (Quinn & Goodman 1986; Quinn, Hernquist, & Fullagar 1993; Tóth & Ostriker 1992) have shown that a merger between a disk galaxy and a satellite having a mass equal to 1/10 of the mass of the disk results in a important thickening of the disk, which is ruled out by observations. However, these simulations ignored the possibility that the satellite might dissolve significantly before the actual merging takes place. More recent simulations (Carlberg 1995; Huang 1995) have suggested that the main effect of these mergers is a tilt of the disk, accompanied by a transient warp, with no substantial thickening.

There are several problems with models involving mergers. Elliptical and spiral galaxies have different globular cluster luminosity functions (Harris 1981). Since merging events would unlikely affect the structure of globular clusters, this result argues against elliptical galaxies being formed from the merging of spirals. Also, dwarf ellipticals presumably do not result from mergers, so the continuity of properties for dwarf ellipticals to regular ellipticals (Sandage 1983) suggests that large elliptical do not result from mergers either. Finally, stars are very strongly concentrated in elliptical galaxies, but not in spirals, and it is not clear how the fusion of two less concentrated systems could lead to the formation of a more concentrated one (Combes et al. 1995).

1.3.3. Initial Conditions

The third class of models comprises models in which the initial conditions are primarily responsible for determining the morphological type of galaxies, with subsequent morphological evolution playing little role or no role at all. Numerous models have been proposed (see Dressler 1984, and references therein), in which the morphological type is determined either by the local density, or the local amount of angular momentum. Such models could successfully explain the observed morphology-density relation only if galaxies have formed near their present location. This could be the case in cosmological models which have more power at large scale than small scale. In such models, clusters would form first, and then fragment into individual galaxies, in which case galaxies could actually be located at present near the location were they where formed. The alternative is that galaxies, at the epoch of their formation, somehow "know" the kind of environment in which they will be located at the present. This can be achieved if there is some kind of coupling between the perturbations responsible for forming the galaxies and the ones responsible for forming the clusters in which these galaxies end up. Such coupling requires non-Gaussian initial conditions.

The problem with these scenarios is that they all invoked cosmological models that are usually considered "marginal." These models constitute interesting alternatives to the more standard CDM or CDM-like models with Gaussian initial conditions, but there is at present no strong, absolute evidence favoring such models over the standard ones. To our knowledge, the most serious alternatives, at present, to the standard CDM models are the models with Cold + Hot Dark Matter (CHDM), models with a nonzero cosmological constant, and models with a tilted power spectrum. None of these cosmological models can achieve the desired effect. Hence, following Dressler (1984), we will regard these types of galaxy formation models as "last resort."

1.4. Past History of Galaxies

In order to identify the correct galaxy formation model, we must reconstruct the past history of the presently observed galaxies, and in particular we need to know the kind of environment in which galaxies were located at various epochs. We are assuming that galaxies at their formation epoch have no knowledge of the future environment in which they will end up. We are therefore rejecting all "class three" models, unless galaxies form near there present location. Hence, if we find that elliptical and S0 galaxies located in the dense cluster cores were always located in high density environment, at all epochs up to the galaxy formation epoch (redshifts z of order 3–5), it would argue in favor of the initial conditions being responsible for determining the morphological type (class three models), and against morphological evolution. If, to the contrary, many of these elliptical and S0 galaxies are found at early time in low density environments, it would argue in favor of morphological evolution (class one or two models). The goal of this paper is to settle this question.

2. THE MODELS

We consider three different cosmological models: an Einstein-de Sitter model with $\Omega_0 = 1$, $\lambda_0 = 0$, an open model with $\Omega_0 = 0.2$, $\lambda_0 = 0$, and a low-density flat model with $\Omega_0 = 0.2$, $\lambda_0 = 0.8$, where Ω_0 and λ_0 are the present values of the density parameter and cosmological constant, respectively. We set the present value H_0 of the Hubble constant equal to $50 \, \text{km/s/Mpc}$ to avoid conflict between the models and the measurements of globular cluster ages. With these parameters, the age of the universe t_0 is 13.0 Gyr, 16.6 Gyr, and 21.04 Gyr for the Einstein-de Sitter, open, and cosmological constant models, respectively.

We assume that the initial fluctuations originate from a Gaussian random process. The initial density contrast can then be expressed as a superposition of plane waves with random phases. Our simulations assume periodic boundary conditions. This restricts the range of possible values for the wavenumber \mathbf{k} to multiples of the fundamental wavenumber $k_0 \equiv 2\pi/L_{\rm box}$, where $L_{\rm box}$ is the size of the computational volume. The density contrast can then be expressed as

$$\delta(\mathbf{x}) = \sum_{\mathbf{k}} \delta_{\mathbf{k}} e^{-i\mathbf{k} \cdot \mathbf{x}}, \qquad (1)$$

where $\delta_{\mathbf{k}}$ is the amplitude of the **k**-mode, and the sum is over all values of $\mathbf{k} = (l, m, n)k_0$, with l, m, n integers. The requirement that $\delta(\mathbf{x})$ is real implies $\delta_{\mathbf{k}} = \delta_{-\mathbf{k}}^*$. The phases of the amplitudes are random, and the norms $|\delta_{\mathbf{k}}|$ are related to the power spectrum P(k) by

$$P(k) = \frac{V_{\text{box}}}{(2\pi)^3} |\delta_{\mathbf{k}}|^2.$$
 (2)

The power spectrum we use can be expressed as

$$P(k) = AkT(k)^2, (3)$$

where A is the amplitude and has dimension of $(\text{length})^4$, and T(k) is the transfer function. This equation describes an "untilted" power spectrum which reduces to the Harrison-Zel'dovich power spectrum $P(k) \propto k$ at large scale, as $T(k) \to 1$ for $k \to 0$. The value of the amplitude is fixed by the value of the cosmic microwave background temperature anisotropy, as measured by COBE (Smoot et al. 1992),

$$A = \frac{1}{(2\pi)^3} \frac{6\pi^2}{5} Q_2^2 R_H^4 \,, \tag{4}$$

where Q_2 is the temperature quadrupole anisotropy and R_H is the radius of the horizon. For all simulations, we used the value $A = 8.16 \times 10^5 h^{-4} \text{Mpc}^4 = 1.3056 \times 10^7 \text{Mpc}^4$ given by Bunn, Scott, & White (1995) for standard CDM models. We also use the transfer function given by Bardeen et al. (1986),

$$T(k) = \mathcal{L}(z) \frac{\ln(1+2.34q)}{2.34q} \left[1 + 3.89q + (16.1q)^2 + (5.46q)^3 + (6.71q)^4 \right]^{-1/4}, \tag{5}$$

where

$$q = \frac{k\theta^{1/2}}{(\Omega_X h^2 \text{Mpc}^{-1})},\tag{6}$$

where Ω_X is the density parameter of the dark matter (non-baryonic) component, $\theta = 1$ for models with 3 flavors of relativistic neutrinos, and $\mathcal{L}(z)$ is the linear growth factor between the initial state and the present, given by

$$\mathcal{L}(z) = \frac{\delta_{+}(0)}{\delta_{+}(z)},\tag{7}$$

where δ_+ is the linear growing mode of the perturbation. Notice that several different notations are commonly used in the literature. Several authors do not include the factor $(2\pi)^3$ in equations (2) and (4), and instead include a factor of $(2\pi)^{3/2}$ in equation (1). Other authors use a redshift-independent transfer function, without the $\mathcal{L}(z)$ factor, and include a factor of $\mathcal{L}^2(z)$ in equation (3).

In all models, we assume that the baryon content of the universe has a density parameter $\Omega_B = 0.0625$. For the Einstein de-Sitter model, this gives a density parameter $\Omega_X = \Omega_0 - \Omega_B = 0.9375$ for the dark matter. For the other two models considered, $\Omega_0 = 0.2$, and therefore Ω_X should be equal to 0.1375, resulting in a shift of the power spectrum through the relation between q and k given by equation (6). Instead, we decided to use the same relationship between k and q for all three models by setting $\Omega_X = 0.9375$ in equation (6), thus introducing an inconsistency. Our motivation for doing this is the following: Our goal is not to find which model fits the observations of the present universe better. Instead, we want to select cosmological models that will bracket the behavior of the large-scale structure formation process. Using for our initial conditions a power spectrum that differs among the various models only through the model-dependent linear growth factor \mathcal{L} allows us to investigate directly the effects of the growth rate and the age of the universe on the evolution of galaxy clustering. In the same spirit, we are considering open models and models with a cosmological constant that are somewhat too extreme to agree with observations, which suggests that Ω_0 is more likely to be somewhere in the range 0.25–0.5 (Ostriker & Steinhardt 1995; Martel, Shapiro, & Weinberg 1997, and references therein). Models with a larger Ω_0 and/or a smaller λ_0 would reproduce observations better, but would resemble the Einstein-de Sitter model more than the ones we are considering, thus providing less insight on the effect of the cosmological parameters on the formation of clusters. The reader should therefore keep in mind that the power spectrum we are using for the open and cosmological constant model is not consistent with a standard CDM model, and is chosen only for practical considerations.

The growing modes $\delta_{+}(z)$ appearing in equation (7) are obtained by solving the linear perturbation equation in the zero-pressure limit. For the Einstein-de Sitter model ($\Omega_0 = 1, \lambda_0 = 0$), the growing mode is

$$\delta_{+}(z) = (1+z)^{-1}. \tag{8}$$

For open models ($\Omega_0 < 1$, $\lambda_0 = 0$), the growing mode is

$$\delta_{+}(z) = 1 + \frac{3}{x} + 3\left(\frac{1+x}{x^3}\right)^{1/2} \ln\left[(1+x)^{1/2} - x^{1/2}\right]$$
(9)

(Peebles 1980), where

$$x = (\Omega_0^{-1} - 1)(1+z)^{-1}. (10)$$

Finally, for flat models with a cosmological constant $(\Omega_0 + \lambda_0 = 1)$, the growing mode is given by

$$\delta_{+}(z) = \left(\frac{1}{y} + 1\right)^{1/2} \int_{0}^{y} \frac{dw}{w^{1/6} (1+w)^{3/2}}$$
(11)

(Martel 1991b), where

$$y = \frac{\lambda_0}{\Omega_0} (1+z)^{-3} \,. \tag{12}$$

3. THE CALCULATIONS

3.1. The P^3M Algorithm

All N-body simulations presented in this paper are done using the *Particle-Particle/Particle-Mesh* (or P³M) algorithm (Hockney & Eastwood 1981; Efstathiou & Eastwood 1981; Efstathiou et al. 1985, hereafter

EDFW). The calculations evolve a system of gravitationally interacting particles in a cubic volume with triply periodic boundary conditions, comoving with Hubble flow. The forces on particles are computed by solving Poisson equation on a $128 \times 128 \times 128$ grid using a Fast Fourier Transform method. The resulting force field represents the Newtonian interaction between particles down to a separation of a few mesh spacings. At shorter distances the computed force is significantly smaller than the physical force. To increase the dynamical range of the code, the force at short distance is corrected by direct summation over pairs of particles separated by less than some cutoff distance r_e . With the addition of this so-called short-range correction, the code accurately reproduces the Newtonian interaction down to the softening length η . In all calculations, η and r_e were set equal to 0.3 and 2.7 mesh spacing, respectively. With these particular values, the code has a dynamical range of three orders of magnitude in length (EDFW). The particular version of P^3M we used in this paper uses the so-called tilde coordinates (Shandarin 1980; Martel & Shapiro 1997). The system is evolved forward in time using a second order Runge-Kutta time-integration scheme with a variable time step. We define a system of units by setting the mass $M_{\rm sys}$ of the system, the comoving side $L_{\rm box}$ of the computational volume, and the gravitational constant G equal to unity.

In all cases, the comoving length of the computational volume is $L_{\rm box} = 128 \rm Mpc$ (present length units). The total mass of the system is $M_{\rm sys} = 3H_0^2\Omega_0L_{\rm box}^3/8\pi G = 1.455\times 10^{17}\Omega_0\rm M_{\odot}$. We use $64^3 = 262,144$ equal mass particles. The mass per particle is therefore $M_{\rm part} = M_{\rm sys}/64^3 = 5.551\times 10^{11} \rm M_{\odot}$ for the Einstein-de Sitter model and $1.110\times 10^{11} \rm M_{\odot}$ for the other two models.

3.2. Initial Conditions

The method we use to set up initial conditions is fairly standard. We lay down $64^3 = 262,144$ particles on a uniform cubic lattice, and displace them from their initial position in order to represent the initial density fluctuations. We then compute the initial peculiar velocities using the linear perturbation solutions for a pure growing mode, which are given by equations (8)–(12).

The particle displacements are given by

$$\Delta \mathbf{x} = -2\sum_{\mathbf{k}} \frac{\delta_{\mathbf{k}} \mathbf{k}}{2\pi k^2} \sin(2\pi \mathbf{k} \cdot \mathbf{x} - \phi_{\mathbf{k}}), \qquad (13)$$

where \mathbf{x} the unperturbed position, $\phi_{\mathbf{k}}$ is a random phase between 0 and 2π , and the sum extends over one half of the \mathbf{k} -volume (the sine function and the factor of 2 come from grouping terms in equation [1] by pairs with equal and opposite wavenumbers). In computational units, k=1 is the fundamental mode, whose wavelength is equal the the size L_{box} of the computational volume, and all modes up to the Nyquist frequency k=32 are included.

To compute the initial peculiar velocity field, we assume that the initial time of the calculation is early enough for the perturbation to be in the linear regime, but late enough so that the linear decaying mode can be neglected. The initial peculiar velocity of the particles are then related to their displacements by

$$\mathbf{v}_i = \frac{\dot{\delta}_+(z_i)}{\delta_+(z_i)} \Delta \mathbf{x} \,, \tag{14}$$

where $\Delta \mathbf{x}$ is computed using equation (10), δ_+ is the linear growing mode of the perturbation, defined by equations (8)–(12), and z_i is the initial redshift of the simulations.

3.3. The Simulations

We ran 5 simulations for each of the three cosmological models, for a total of 15 simulation. For each model, the 5 simulations differ only in the ensemble of random phases used in equation (13) to generate the initial particle displacements. To identify these various simulations, we shall use the following nomenclature: The simulations for the Einstein-de Sitter model ($\Omega = 1$, $\lambda_0 = 0$), the open model ($\Omega_0 = 0.2$, $\lambda_0 = 0$), and cosmological constant model ($\Omega_0 = 0.2$, $\lambda_0 = 0.8$) will be called EdSX, OX, and LX, respectively, where X = 1, 2, 3, 4, 5 identifies the various runs for each model. All simulations start at an initial redshift $z_i = 24$, and end at z = 0.

4. THE PRESENT GALAXY DISTRIBUTIONS AND MORPHOLOGICAL TYPES

4.1. The Galaxy Locations

The P³M algorithm simulates the growth of density fluctuations resulting in the formation of large-scale structure in an expanding universe. The only physical interaction present in these simulations is gravity. Hence, all the hydrodynamical and radiative processes which certainly play an important role in the galaxy formation process are ignored. Various authors have used P³M codes to simulate galaxy formation, either by using a static (Davis et al 1985) or dynamic (Martel 1991a) criterion for identifying "luminous" particles, by making particles "stick" to each others in order to simulate dissipation of kinetic energy by hydrodynamical processes (Carlberg 1988), or by combining the P³M algorithm with a hydrodynamical algorithm such as Smoothed Particles Hydrodynamics (Evrard 1988). In our simulations, we use a much simplier approach. We consider the large-scale structure at present (z = 0) resulting from the P³M simulations, and design an empirical Monte-Carlo method for locating galaxies in the computational volume, based on the constraints that (1) galaxies should be predominantly located in the densest regions, and (2) the resulting distribution of galaxies should resemble the observed distribution on the sky.

One possibility consists of using a Monte-Carlo rejection method. We could generate locations at random inside the computational volume, and decide whether or not to put a galaxy in these location, based on the local density of matter. The likelihood of locating a galaxy in a particular location should not be a linear function of the local density, however. Galaxy formation is believed to be biased toward forming galaxies in high density regions (Kaiser 1984). So in order to use this method, we would need to know the precise relationship between the matter density and the likelihood of forming a galaxy. The best currently available theories for biased galaxy formation could provide such a relationship, but using this relationship for locating galaxies would be an overkill. Biased galaxy formation theories could only provide relationships that involve the actual matter distribution in the universe. We are dealing instead with a simulated matter distribution, which is only an approximation of the actual matter distribution. In particular, CDM models normalized to COBE are known to produce too much structure on small scales.

Considering these various difficulties, we chose a much simpler method for locating galaxies. We divide the present computational volume into 128^3 cubic cells of size 1Mpc^3 , and compute the matter density ρ at the center of each cell, using the same mass assignment as in the P^3M code. We then choose a particular density threshold ρ_t . We locate N galaxies in each cell, where N is given by

$$N = \operatorname{int}\left(\frac{\rho}{\rho_{t}}\right). \tag{15}$$

The actual location of each galaxy is chosen to be the center of the cell, plus a random offset of order of the cell size. This eliminates any spurious effect introduced by the use of a grid. We then experiment with various values of the density threshold ρ_t until the total number of galaxies comes out to be of order 40000. This gives a number density of ~ 0.02 galaxies/Mpc³.

In Figure 1, we take one simulation for each of the three models, and plot the location at z=0 of the P³M particles (left panels) and the galaxies (right panel) inside a slice of size $128 \times 128 \times 8$ Mpc. The Einstein-de Sitter model has too much power on small scales, resulting in the formation of very dense clumps. The cosmological constant model is slightly less evolved, and shows a large number of average-size clusters that have not yet merged into larger ones as in the Einstein-de Sitter model. In this model, the small value $\Omega_0 = 0.2$ of the density parameter results in a small growing rate of the density fluctuations, but this effect is partly compensated by the presence of the cosmological constant λ_0 , which increases the age of the universe and thus allows the fluctuations to grow for a longer period of time. The open model O1 forms significantly less structure than the other two.

The galaxies are mostly concentrated in the highest density regions. The use of a density threshold in equation (15) approximates quite well the effect of biased galaxy formation by not locating galaxies in low density regions. The galaxy distribution for the open model resembles the observed galaxy distribution. The galaxies in the other 2 models are too much clustered. To quantify this point, we compute the 2-point correlation function $\xi(r)$ from the simulated galaxy distributions, for the Einstein-de Sitter and open models (we omitted the cosmological constant model for clarity). The results are shown in Figure 2. The correlation function for the open model (triangles) matches the observed power law $\xi(r) = (r/5.4h^{-1}\text{Mpc})^{-1.77}$ (Peebles 1993) (dotted line), for separations 4 Mpc < r < 40 Mpc. The correlation function for the Einstein-de Sitter model (filled circles) is too large by a factor of 3 over the same range. This is consistent with results obtained by various authors who have used more sophisticated methods for generating galaxy distributions (see Ostriker 1995, and references therein). Hence, the overclustering of galaxies in our Einstein-de Sitter model should not be regarded as a flaw in our empirical method for locating galaxies, but rather as a weakness of the CDM model normalized to COBE. We attribute the excess of correlation at separations r < 4 Mpc for the open model to the same overmerging problem.

Since there is too much galaxy clustering at present in our Einstein-de Sitter model, we can expect that earlier time slices will resemble observations better than the present ones. Using linear perturbation theory, we can approximate the evolution of the correlation function as $\xi[r/(z+1),z]\approx (1+z)^{-2}\xi(r,z=0)$. Since the correlation function for the Einstein-de Sitter model is too large by a factor of 3 at z=0, this relation predicts that the $z=3^{1/2}-1\sim0.7$ time slice should match observations better than the present time slice, which is indeed the case, as shown by the open circles in Figure 2.

4.2. The Morphological Types

As we mentioned in §1.1, there is a tight relation between the distribution of morphological types and the number density of galaxies (Dressler 1984, and references therein). This morphology-density relation is reproduced in Figure 3, by the solid curves. By combining this relation with a Monte-Carlo method, we can ascribe a morphological type to each galaxy, as follows. We first compute the volume number density of galaxies $\rho_{\rm gal}$ around each galaxy, using

$$\rho_{\rm gal} = \frac{n+1}{4\pi d_n^3/3}\,,\tag{16}$$

where n is a positive integer, and d_n is the distance of the n^{th} nearest neighboring galaxy. In all cases, we choose n = 12. In the case of a spatially uniform distribution of galaxies with a density ρ_{uniform} , this formula gives the correct answer $\rho_{\text{gal}} \approx \rho_{\text{uniform}}$ for a galaxy located inside the distribution, and $\rho_{\text{gal}} \approx \rho_{\text{uniform}}/2$ for a galaxy located at the edge of the distribution, since that galaxy has neighbors on one side only. Notice the Dressler (1980) used essentially the same technique to compute the surface number density of galaxies around each galaxy in his sample.

Once the densities are computed, we compute the fractions $f_{\rm Sp}(\rho_{\rm gal})$, $f_{\rm S0}(\rho_{\rm gal})$, and $f_{\rm Ell}(\rho_{\rm gal})$ from the morphology-density relation. We then ascribe a morphological type to each galaxy by generating a random number x between 0 and 1 (with uniform probability). The galaxy is a spiral if $x < f_{\rm Sp}$, a S0 if $f_{\rm Sp} < x < f_{\rm Sp} + f_{\rm S0}$, and an elliptical if $x > f_{\rm Sp} + f_{\rm S0}$. Table 1 shows the percentages of galaxies of each type for each run. Notice that the fluctuations among different runs within each model are very small. The fluctuations among different models are larger, and reflect the differences in the amount of clustering at z = 0. As we see in Figure 1 (left panels), there is more clustering in the Einstein-de Sitter model than in the cosmological constant model, and significantly more in these two models than in the open model. This results in a slight excess of elliptical and S0 galaxies in the Einstein-de Sitter model compared to the cosmological constant model, and a bigger excess in these two models compared to the open one.

Once the morphological types have been assigned, we can compute the resulting morphology-density relation, and compare it to the one we were attempting to reproduce. Figure 3 shows the results for the EdS runs. The error bars indicate the range of values amongst the 5 different runs for that model, with the symbols indicating the results obtained by combining all runs together (this is not the same as the average among the runs, since the various runs contain different numbers of galaxies). The results reproduce the desired relations quite well, except at the largest density, where small number statistics lead to large fluctuations.

5. TRACING GALAXIES BACK IN TIME

The P³M algorithm provides us with the distributions of particles at various intermediate redshifts between the initial redshift z = 24 and final redshift z = 0. By combining these particle distributions with our simulated galaxy distributions at present, we can trace galaxies back in time and reconstruct their trajectory. To do this, we simply find the nearest particle $p_i^{(1)}$ of each galaxy g_i at present. Then we "tie" the galaxy g_i to that nearest particle. The location of the galaxy q_i at any redshift z is then given by:

$$\mathbf{r}[g_i, z] = \mathbf{r}\left[p_i^{(1)}, z\right] + \mathbf{r}', \tag{17}$$

where \mathbf{r}' is a small random offset, which we introduce to avoid the unfortunate situation of having two galaxies located at the top of each other because they happen to by tied to the same particle. This allows us to construct galaxy distributions at any redshift, and, more importantly, to follow the history of each galaxy as cluster formation and merging is taking place. Of course, if we trace galaxies back to redshifts larger than 3–5, we then end up, strictly speaking, with distributions of *protogalaxies*. In Figure 4, we plot the galaxies located inside a slice of comoving thickness 32Mpc (that is, one quarter of the computational volume) at various redshifts, for the run EdS1.

6. MORPHOLOGICAL EVOLUTION

6.1. Elliptical Galaxies

Knowing the location of each galaxy at various epoch, we can then study the local environment in which each galaxy is located, and how this environment evolves with time. The basic idea is the following: If elliptical galaxies located in the dense cores of clusters at z=0 were always located in high density environment, it will argue against morphological evolution, and suggest that galaxies formed in such high density environment form predominantly as ellipticals. If on the contrary, many of these elliptical galaxies were located in low density environment at, say, z=3, it will argue in favor of morphological evolution, with these galaxies forming as spiral and later on becoming elliptical as they find themselves in high density environment.

To investigate this question, we compute the number density of galaxies around each galaxy for all 15 runs (3 models with 5 runs for each), at z=0 and z=3, using the method described in §4.2. We are making the null hypothesis that there is no morphological evolution, hence an elliptical at z=0 is also elliptical at z=3. We then sort each list of ~ 40000 galaxies in increasing order of the local number density of galaxies.

First, we divide galaxies into low-density environments (L) and high-density environments (H), both at z=0 and z=3, based on the median value of the density at that epoch. That is, each list contains ~ 20000 galaxies in low-density environments and the same number in high-density environments. We then divide galaxies into 4 bins according to the type of environments (L or H) in which they are located at z=3 and z=0. The results are shown in Table 2, where the L \rightarrow L bin contains all elliptical galaxies located in low-density regions at z=3 and high-density regions at z=0, and so on. By definition the L \rightarrow H and H \rightarrow L counts are equal if all galaxies are considered, but for now we are only considering elliptical galaxies.

These results show that galaxies are moving through environments of different number densities between z=3 and z=0. In the Einstein-de Sitter model (runs EdS1 – EdS5), for instance, only 70% of the ellipticals are either L \rightarrow L or H \rightarrow H. The numbers are very similar among different runs within each model, showing that these results are statistically significant. In all cases, the L \rightarrow H count exceeds the H \rightarrow L count. In order to appreciate the significance and implications of this result, let us consider a simple, probabilistic model in which the probability that an elliptical galaxy is located in similar environments at z=3 and z=0 is 1/2+p. We obtain the following relations:

$$H_0 = H_3\left(\frac{1}{2} + p\right) + L_3\left(\frac{1}{2} - p\right),$$
 (18)

$$L_0 = L_3 \left(\frac{1}{2} + p\right) + H_3 \left(\frac{1}{2} - p\right),$$
 (19)

where H_z and L_z , z=0,3 are the number of elliptical galaxies in high- and low-density environments, respectively, at redshift z. This model has two extreme and opposite limits, which we shall refer to as the "no mixing limit" and the "complete mixing limit." In the no mixing limit, defined by p=1/2, each galaxy is located at present at or very near the location (in comoving coordinates) where it was initially formed. Galaxies are therefore in identical environments at z=3 and z=0, and furthermore, they have the same neighbors. In the complete mixing limit, defined by p=0, all memory of the location where galaxies were formed has been lost through chaotic mixing. Any given galaxy can end up at present either in a low- or high-density environment, with equal probability, no matter in which kind of environment it was formed. In this limit, $H_0 = L_0$, so if the number of galaxies in high- and low-density environments at present is actually different, there is a finite minimum probability p_{\min} . We refer to the case $p=p_{\min}$ as the "maximum mixing

limit." We can use this model to analytically compute the $L \to H$ and $H \to L$ counts and compare them to the ones given in Table 3, as follows: We assume that the distribution of galaxies are known at present, but instead of tracing these galaxies back in time, we now use equations (18) and (19) to compute the galaxy distributions at z = 3, we get

$$H_3 = \frac{H_0(1/2+p) - L_0(1/2-p)}{2p}, \qquad (20)$$

$$L_3 = \frac{L_0(1/2+p) - H_0(1/2-p)}{2p}. (21)$$

by imposing that H_3 and L_3 are nonnegative, we can solve for the minimum probability,

$$p_{\min} = \frac{|\mathbf{H}_0 - \mathbf{L}_0|}{2(\mathbf{H}_0 + \mathbf{L}_0)}.$$
 (22)

Equations (20) and (21) can be solved for any value of p between p_{\min} (maximum mixing limit) and 1/2 (no mixing limit). The L \rightarrow H and H \rightarrow L counts are then given by $L_3(1/2-p)$ and $H_3(1/2-p)$, respectively. We plot the results as a function of p in Figure 5, for all three cosmological models (the values of H_0 and L_0 used in equations [20] and [21] were obtained by averaging over all five runs within each model).

In all cases, the L \rightarrow H count is lower than the H \rightarrow L count, for all values of p. The cases $p=p_{\min}$ and p=1/2 constitute two extreme and opposite limits, no mixing and maximum mixing, and interestingly these two extreme limits do not bracket our results. The reason is that an excess of L \rightarrow H count over H \rightarrow L count should not occur "naturally" unless there are more galaxies in low-density environments than in high-density environments at z=3, which is clearly not the case for ellipticals in our simulations.

This seemingly absurd result is based on the assumption that there is no morphological evolution. If we relax this assumption, we can solve the "L \rightarrow H excess" problem. If some elliptical galaxies located in high-density environments at present were actually formed as spiral galaxies in low-density environments, and eventually became ellipticals as they found themselves in higher-density environments at later time, then we are overestimating the L \rightarrow H count by ignoring morphological evolution. In order to bring the L \rightarrow H count down to the value of the H \rightarrow L count or lower, we must speculate that at least 1/4 of the elliptical galaxies in the L \rightarrow H bin were formed as spiral galaxies, and underwent morphological evolution between z=3 and z=0 that transformed them into elliptical galaxies.

6.2. All Morphological Types

In this subsection, we consider galaxies of all types (not only ellipticals) that have formed in low-density environments. The results are shown in Table 3, where the numbers in parentheses are the percentages for each type. We are still making the null hypothesis of no morphological evolution. The percentages are different for the $L \to L$ and $L \to H$ bins, which is of course totally absurd: It implies that, somehow, the galaxy formation process is able to "distinguish" a low density environment at z=3 that will remain low-density at all times from one that will eventually become high-density. Since we assume there is no "fortune teller" at z=3 that can "tell" the galaxy formation process what will happen in the future, thus excluding class 3 models, we must conclude that morphological evolution is present. We can reconcile the numbers presented in Table 3 by assuming that spiral galaxies evolve either into S0 or ellipticals galaxies. For instance, we can reconcile the percentages for the EdS1 run by "transferring" 534 galaxies from the

 $L \to H$ S0 bin to the $L \to H$ Spiral bin, and 159 galaxies from the $L \to H$ Elliptical bin to the $L \to H$ Spiral bin. The percentages would then be the same as for the $L \to L$ bins. This would imply that 21% of these S0 galaxies (534 out of 2565) and 17% of these elliptical galaxies (159 out of 924) were formed as spiral galaxies and underwent morphological evolution at a later time.

One possible problem with this interpretation of the results is our definition of low-density and high-density environments. At z=3, for the Einstein-de Sitter model, the number density of galaxies around each galaxy varies from 1.3×10^3 to 2.6×10^7 per unit computational volume with the median being 2×10^5 (the comoving number density is obtained by dividing these numbers by $[128\,\mathrm{Mpc}]^3$; the physical number density is obtained by dividing these numbers by $[128(1+z)^{-1}\,\mathrm{Mpc}]^3$). Hence, the number density in "low density environments" defined as the bottom half of the distribution, varies over 2 orders of magnitude. Then we could argue that the galaxies ending up in low- and high-density environments at z=0 come from different "parts" of the low-density environments at z=3.

To solve this problem, we define a "very low density" (VL) environment, comprising all galaxies located in the bottom 1/20 of the number density distribution, that is, the ~ 2000 of these ~ 40000 galaxies that are located in the least dense environments. The number density at z=3 around these galaxies varies from 1.3×10^3 to 2.8×10^4 , but if we ignore a small number of galaxies in extremely low density environments (about 50), the range becomes $5.0 \times 10^3 - 2.8 \times 10^4$. The physical conditions for galaxy formation in these regions should be quite uniform, hence the percentages of spirals, S0's, and ellipticals should be essentially the same everywhere within these regions. We then look at the location of these galaxies at z=0. The results are shown in Table 4.

Again, these percentages are different depending on whether the galaxies end up in low- or high-density environments at z=0 (the results for the open models are statistically insignificant, because only 10 galaxies ended up in high-density environments). Since the galaxy formation process cannot predict which galaxies will end up in high or low-density environments at z=0, we are forced to reject the null hypothesis of no morphological evolution.

Again, we can reconcile the numbers presented in Table 4 by "transferring" galaxies from the $VL \to H$, S0 and Elliptical bins to the $VL \to H$ Spiral bin. By transferring 23 galaxies from the $VL \to H$ S0 bin to the $VL \to H$ Spiral bin, and 5 galaxies from the $VL \to H$ Elliptical bin to the $VL \to H$ Spiral bin, the percentages would become the same as for the $VL \to L$ bins. Hence, 28% (23 out of 82) of these S0 galaxies and 17% (5 out of 30) of these elliptical galaxies formed as spiral galaxies. Notice the similarity of these percentages with the ones computed from Table 3.

These numbers are smaller if we assume that morphological evolution involves galaxy collision and merging. In the simpliest case, morphological evolution transforms 2 interacting spiral galaxies into one S0 or elliptical galaxy. Hence, for each S0 or elliptical galaxy we "remove" from their $VL \rightarrow H$ bin, we need to add 2 spiral galaxies, instead of only one, to the Spiral bin. In this case, to reconcile the percentages for the EdS1 run, we need to remove 18 S0 galaxies and 2 elliptical galaxies, thus adding 40 spiral galaxies $(2 \times [18+2])$. The fractions of S0 and elliptical galaxies that were formed by mergers then becomes 22% (18 out of 82) and 7% (2 out of 30).

7. THE EVOLUTION OF CLUSTERING

The results of the previous section suggest that some elliptical and S0 galaxies were formed as spiral galaxies and underwent morphological evolution at some epoch between redshifts of z=3 and z=0. Assuming that the morphological evolution process is triggered by an increase is the galaxy number density resulting from the formation and merging of clusters, we can attempt to estimate the epoch of galaxy evolution by monitoring the evolution of the number density of galaxies around the galaxies that might have undergone such morphological evolution.

In Figure 6, we plot, as a function of redshift, the number density n of galaxies (in galaxies/Mpc³) around each elliptical galaxy located in the VL \rightarrow H bin of Table 4 (runs O2, O4, and O5 do not contain any such galaxy, and are therefore omitted). The number of curves in each panel can be read from the last column of Table 4. All panels show a similar pattern. Initially, the number density decreases with time, indicating that these regions are still expanding (though slower than Hubble flow). The number densities reach a minimum at epochs between z=0.4 and z=0.8, indicating that the regions surrounding these galaxies have finally turned back and started to recollapse. The number densities then increase by 2 to 3 orders of magnitude between the turnaround epoch and the present, except for the open model (runs O1 and O3) for which the density increase is smaller than one order of magnitude. Some galaxies in the EdS runs (and also one in the L3 run) follow a different history, with the number density starting to rise at $z \sim 1$, then dropping and rising again. The initial increase is caused by the formation of a dense cluster at $z \sim 1$, resulting from the collapse of a particularly large density fluctuation. The subsequent drop in number density is caused by the tidal disruption of that cluster by more massive clusters formed at later epochs. These cases constitute a minority.

These plots indicate that the morphological evolution process, if real, most probably takes place at redshifts smaller than z=0.6, after the number density of galaxies has started to increase. Furthermore, the number densities reach the same value they had at z=3 at a redshift of order $z\sim0.2$. It is tempting to argue that, for morphological evolution to occur, the number density has to get larger than it was at the galaxy formation epoch, and therefore it must occur between z=0.2 and z=0. This argument is not valid because it assumes that the morphological evolution process depends directly on the number density of galaxies, which is presumably not the case. If morphological evolution results from galactic collisions or tidal stripping, then the likelihood for this process actually happening will depend upon the probability of having close encounters between galaxies, which is larger in regions of high number density. However, for the same number density, the likelihood of having close encounters between galaxies is much larger at z=0.2 than at z=3. Not only are galaxies more clustered at z=0.2 (see Fig. 4 for a good illustration of that), but in addition the galaxies, overall, are moving apart from one another at z=3, whereas they are approaching each other at z=0.2. Hence, we cannot rule out the possibility that morphological evolution takes place between redshifts z=0.8 and z=0.2 on the basis that the number densities at these epochs are smaller than they are at z=3.

Several authors have claimed that merging events were more frequent in the past, based either on observations (see, e.g. Carlberg 1995 and references therein) or analytical arguments (Toomre 1977; Aarseth & Fall 1980). These results do not contradict our claim that morphological evolution does not occur at redshifts z > 0.8, simply because we are focusing our attention to very low density regions. In particular, the analytical arguments aforementioned assume that merging involves pairs of galaxies which are already on bound orbits, which is clearly not the case in the regions we are considering, which are still dominated by an overall expansion at z = 3. Also, galaxy merging is only one of many physical processes that could possibly

result in morphological evolution. In this section, we are making no assumption on the nature of the actual physical process involved. We are merely arguing that morphological evolution in very low density regions does not occur until $z \sim 0.8$, simply because at earlier time all galaxies in these regions are moving away from one another.

8. DISCUSSION OF THE METHOD

In this section, we review and discuss the strengths and weaknesses of our numerical simulations, and the interpretation of the results.

8.1. Weak Points

The weakest point of this entire work is certainly the cosmological simulations themselves. The Einsteinde Sitter model with CDM spectrum normalized to COBE is known to produce too much structure at small scale. This is reflected in the two-point correlation function which is too large by a factor of 3 in the range of 1-10 Mpc. Only in the open model does the distribution of galaxies actually resemble the present universe. Since the 2-point correlation function evolves roughly as $a(t)^2 \propto (1+z)^{-2}$ in the linear regime, we can estimate that $z \sim 0.7$ (that is, $3^{1/2}-1$) time-slices for these models would be a better representation of the actual present universe. We looked at these time-slices, and they indeed resemble the present universe more closely than the z=0 time-slice.

It is difficult to estimate the consequences of this excess of small-scale structure. We argue that the effect is not so significant, and does not affect our conclusion. The main point is that we get consistent results among all three models, including the open model which does reproduce the present universe fairly well. Also, it is hard to see how the excess of structure formation in the Einstein-de Sitter model and the cosmological constant model could possibly affect the conclusion. Cluster merging happens continuously in CDM models, all the way to the present. The excess of power simply increases the amount of merging taking place between z=0 and z=3. We divide the regions in which galaxies end up at z=0 into low density and high density environment, without taking into account how high the number density gets inside these regions of high density. Hence, late cluster mergers are unlikely to have a strong effect on the results shown in Tables 2–4. As long as we are not interested in galaxies located in "very high density environments" at z=0, the excess of structures at small scale is probably unimportant.

We traced the motion of galaxies back in time by following the motion of the nearby dark matter particles. This assumes that the velocity field of galaxies and dark matter are the same. This assumption is certainly valid at early times. However, numerical simulations (Carlberg 1994) have shown the existence of a velocity bias between galaxies and dark matter inside clusters of galaxies. This is the result of an evolutionary process taking place inside the clusters. Hence, our method for tracing galaxies back in time might be partly flawed if this velocity bias is real.

8.2. Strong Points

The strongest point of this entire work is that the conclusions do not depend on the details of the initial galaxy formation and morphological evolution processes. The only assumptions we make concerning the

initial galaxy formation process are that (1) it takes place before z=3, and (2) it has no "knowledge" of the future. As for the morphological evolution process, the only assumptions we make are that it converts spiral galaxies into S0 and elliptical galaxies, but not the other way around, and that it takes place in high density environments. The detailed physical processes involved in the initial galaxy formation and morphological evolution processes are irrelevant to this work, and this only makes our results more robust.

The second strongest point is the consistency of our results, first among different simulations for a same cosmological model, and then among the various models. The percentages shown in Tables 3 and 4 (with the exception of the Open model on Table 4) have error bars much smaller than the differences among these various percentages, which is what our argument is based on. Also, the fact that all three cosmological models show a trend toward morphological evolution strongly suggests that this effect is real.

There is a potential problem with the technique we use for tracing galaxies back in time. If dense clusters form by assembling matter taken from distant regions of the universe (which might be the case when cluster mergers are involved), then our approach of tying each galaxy to the nearest dark matter particle becomes ambiguous. A given galaxy might have formed in any of these distant regions, and by following the trajectory of the nearest dark matter particle, we are "forcing" that galaxy to have formed in one particular region, when it could actually have formed in another one.

To estimate the importance of this effect, we go back to the run EdS1, 5 and recompute the trajectories of the galaxies, except that we replace $p_i^{(1)}$, the nearest dark matter particle to each galaxy, by $p_i^{(2)}$, the second-nearest particle, in equation (17). We label this new calculation EdS1*. In Figure 7a, we plot the x-coordinate, in computational units, of the galaxies at z=3 for the EdS1* run, versus the same coordinates for the EdS1 run. Even though there is some scatter, most galaxies are located near the diagonal, indicating that the differences between the two runs are small for most galaxies (the concentrations of galaxies in the upper left and lower right corners of the figure are an artifact of the periodic boundary conditions). Plots of the y- and z-coordinates are similar. For brevity, we are omitting them in this paper.

Figure 7b shows an histogram of the 3-dimensional separation, in computational units, between each galaxy at z=3 in the EdS1 run and its counterpart in the EdS1* run. More than 1/3 of the galaxies are located in the first bin, having separations less than 1/40 [corresponding to a physical separation of $128 \,\mathrm{Mpc}(z+1)^{-1}/40 = 800 \,\mathrm{kpc}$], and the first seven bins contain 92% of the galaxies. Hence, only a few galaxies end up in significantly different regions when we track the second-nearest particle instead of the first one.

Using the galaxy locations for the run EdS1*, we perform the same analysis as for the other runs. The results are given in the last line of Table 4. The numbers for the run EdS1* are remarkably similar to the ones for the EdS1 run. The most important difference is in the fraction of elliptical galaxies in the VL \rightarrow H bin, which is 30% in one case and 42% in the other. But actually, the EdS1* run is closer to the average amongst EdS runs than the EdS1 run is. Therefore, following the trajectory of the second-nearest particle instead of the nearest one does not affect our final conclusion in any way.

⁵We choose a run from the EdS model because the structures are more evolved in this model than in the other ones, with more cluster merging happening at late time. Hence, the effect we are trying to measure is likely to be more important in this model.

9. CONCLUSION AND PROSPECTS

We conclude that a small but non-negligible fraction (of order 10%-20%) of the S0 and elliptical galaxies we observe today in the dense parts of clusters were not formed as S0's and ellipticals, but rather as spiral galaxies, and underwent morphological evolution between z=3 and z=0, presumably during cluster formation and merging. Since the fraction of galaxies involved in morphological evolution is neither 0% nor 100%, initial conditions and morphological evolution processes must both play an important role in determining the morphological type of galaxies.

Our simulations predict that the proportion of spiral galaxies should increase form the present observed value of $\sim 50\%$ to larger values as one looks back in time, that is, at larger redshifts. However, they cannot predict at what redshift this effect would manifest itself. To make a theoretical prediction, we need first to understand the details of the morphological evolution process. Also, the epoch of galaxy formation most certainly depends upon the cosmological model, so before we can make quantitative predictions, we first need to settle the question of which cosmological model properly describes the formation of large-scale structures in the universe.

However, a large amount of observational evidence supporting the existence of morphological evolution in dense environments at redshifts z < 0.5 has been accumulated in recent years. Butcher & Oemler (1978, 1984) discovered a large excess of blue objects in clusters located at redshift $z \geq 0.4$. Subsequent groundbased observations (Dressler & Gunn 1982, 1983; Couch et al. 1983; Couch & Newell 1984; Dressler, Gunn, & Schneider 1985; Ellis et al. 1985; Lavery & Henry 1986; Henry & Lavery 1987; Couch & Sharples 1987; MacLaren, Ellis, & Couch 1988; Soucail et al. 1988; Aragón-Salamanca, Ellis, & Sharples 1991; Aragón-Salamanca et al. 1993) have shown that this "Butcher-Oemler effect" results from short-lived bursts of star formation affecting a subset of the cluster members. These starbursts could be triggered by the ram pressure of the intracluster gas when a galaxy first enters the cluster, by violent interaction between galaxies, or by mergers, (see Bothun & Dressler 1986, and references therein; Oemler 1992, and references therein; Mihos & Hernquist 1994a, 1994b). Recent Hubble Space Telescope observations of high redshifts clusters $z \sim 0.3-0.5$ revealed that the blue starburst objects are low luminosity spiral galaxies, with as many as $\sim 50\%$ of them being disturbed by what appears to be either tidal disruption or merging (Dressler et al. 1994a, 1994b; Couch et al. 1994; Barger et al. 1995). The galaxy populations of these clusters differ significantly form the ones of nearby clusters, and resemble the ones seen in the nearby small groups and field.

The difference between the galaxy populations of high-redshift and low-redshift clusters and the importance of dynamical interaction in high-redshift clusters compared to low-redshift ones provide strong evidence that morphological evolution has occurred inside rich clusters. Studies of galaxy populations in the field (Colless et al. 1990; Griffiths et al. 1994; Mobasher et al. 1996) and in small groups (Allington-Smith et al. 1993), reveal that no significant morphological evolution has occurred in these environments between redshift z=0.5 and the present, at least among luminous galaxies. (Driver et al. [1995], however, found an excess of faint late type galaxies in the field.) These results rule out any model in which the morphological evolution of a galaxy is driven by an internal physical process. The morphological evolution process depends upon the richness of the environment, and thus results in a steepening of the morphology-density relation with time.

The most recent studies (Dressler & Smail 1996, and references therein) of high-redshift clusters, which include 10 rich clusters (0.36 < z < 0.56) comprising ~ 2000 galaxies, show that the excess of spiral galaxies in high-redshift clusters is compensated by an underabundance of S0 galaxies, but not ellipticals. This

implies that if morphological evolution is responsible for forming both some S0 and some elliptical galaxies, as our numerical simulations suggest, then the process of converting spirals galaxies into ellipticals must have occurred before z=0.56. This hypothesis constitutes an observational challenge, since testing it requires observations of even more distant clusters, in the range $z\sim0.5-0.8$, and a theoretical challenge as well, finding a model that explains why morphological evolution produces S0 and elliptical galaxies at different epochs.

All these observational results are consistent with our conclusion that a fraction of the elliptical and S0 galaxies result from morphological evolution processes taking place between redshifts of order unity and the present. The observations and our numerical simulations both indicate that the correct galaxy formation model ought to be a "class two" model, in which both initial conditions and morphological evolution play an important role. Finding the correct galaxy formation model will most likely require a better understanding of the physical processes involved and the cosmological context in which they are taking place, as well as observations and determination of morphological types in clusters beyond redshift $z \sim 0.5$.

This work benefited from stimulating discussions with Alan Dressler, Inger Jørgensen, George Lake, and Paul Shapiro. We are pleased to acknowledge the support of NASA Grant NAG5-2785, NSF Grants PHY93 10083 and ASC 9504046, the University of Texas High Performance Computing Facility through the office of the vice president for research, and Cray Research.

REFERENCES

Aarseth, S. J., & Fall, S. M. 1980, ApJ, 236, 43

Allington-Smith, J. R., Ellis, R. S., Zirbel, E. L., & Oemler, A. 1993, ApJ, 404, 521

Aragón-Salamanca, A., Ellis, R. S., Couch, W. J., & Carter, D. 1993, M.N.R.A.S., 262, 764

Aragón-Salamanca, A., Ellis, R. S., & Sharples, R. M. 1991, M.N.R.A.S., 248, 128

Bardeen, J. M., Bond, J. R., Kaiser, N., & Szalay, A. S. 1986, ApJ, 304, 15

Barger, A. J., Aragón-Salamanca, A., Ellis, R. S., Couch, W. J., Smail, I., & Sharples, R. M. 1995, M.N.R.A.S., 279, 1

Barnes J. E. 1989, Nature, 338, 123

Barnes, J. E., & Hernquist, L. 1991, ApJ, 370, L65

Barnes, J. E., & Hernquist, L. 1992, Nature, 360, 715

Baugh, C. M., Cole, S., & Frenk, C. S. 1996, M.N.R.A.S., 282, L27

Bhavsar, S. P. 1981, ApJ, 246, L5

Biviano, A., Durret, F., Gerbal, D., Le Fèvre, O., Lobo, C., Mazure, A., & Slezak, E. 1995, A&A, 297, 610

Bothun, G. D., & Dressler, A. 1986, ApJ, 301, 57

Bothun, G. D., Schommer, R. A., & Sullivan, W. T. 1982, M.N.R.A.S., 87, 731

Bunn, E. F., Scott, D., & White, M. 1995, ApJ, 441, L9

Butcher, H., & Oemler, A. 1978, ApJ, 219, 18

Butcher, H., & Oemler, A. 1984, ApJ, 285, 426

Byrd, G., & Valtonen, M. 1990, ApJ, 350, 89

Carlberg, R. G. 1988, ApJ, 332, 26

Carlberg, R. G. 1994, ApJ, 433, 468

Carlberg, R. G. 1995, in Galaxies in the Young Universe, eds H. Hippelein, et al. (New York:Springer), p. 207

Colless, M., Ellis, R. S., Taylor, K., & Hook, R. N. 1990, M.N.R.A.S., 244, 408

Combes, F., Boissé, P., Mazure, A., & Blanchard, A. 1995, in Galaxies and Cosmology (New York:Springer) pp. 202–204

Couch, W. J., Ellis, R. S., Godwin, J., & Carter, D. 1983, M.N.R.A.S., 262, 764

Couch, W. J., Ellis, R. S., Sharples, R. M., & Smail, I. 1994, ApJ, 430, 121

Couch, W. J., & Newell, E. B. 1984, ApJ, 56, 143

Couch, W. J., & Sharples, R. M. 1987, M.N.R.A.S., 229, 42

Cowie, L. L., & Songaila, A. 1977, Nature, 266, 501

Davis, M., Efstathiou, G., Frenk, C. S., & White, S. D. M. 1985, ApJ, 292, 371

de Souza, R. E., Capelato, H. V., Arakaki, L., & Logullo, C. 1982, ApJ, 263, 557

Dressler, A. 1980, ApJ, 236, 351

Dressler, A. 1984, Ann.Rev.A.A. 22, 185

Dressler, A., & Gunn, J. E. 1982, ApJ, 263, 533

Dressler, A., & Gunn, J. E. 1983, ApJ, 270, 7

Dressler, A., Gunn, J. E, & Schneider, D. P. 1985, ApJ, 294, 70

Dressler, A., Oemler, A., Butcher, H. R., & Gunn, J. E. 1994a, ApJ, 430, 107

Dressler, A., Oemler, A., Sparks, W. B., & Lucas, R. A. 1994b, ApJ, 435, L23

Dressler, A., & Smail, I. 1996, preprint astro-ph/9611004

Driver, S. P., Windhorst, R. A., Ostrander, E. J., Keel, W. C., Griffiths, R. E., & Ratnatunga, K. U. 1995, ApJ, 449, L29

Efstathiou, G., Davis, M., Frenk, C. S., & White, S. D. M. 1985, ApJS, 57, 241

Efstathiou, G., & Eastwood, J. W. 1981, M.N.R.A.S., 194, 503

Efstathiou, G., & Jones, B. J. T. 1979, M.N.R.A.S., 186, 133

Ellis, R. S., Couch, W. J., MacLaren, I., & Koo, D. C. 1985, M.N.R.A.S., 217, 239

Evrard, A. E. 1988, M.N.R.A.S., 235, 911

Fall, S. M. 1979, Nature, 281, 200

Geller, M. J., & Beers, T. C. 1982, PASP, 94, 421.

Gerhard, O. E. 1981, M.N.R.A.S., 197, 179

Giovanelli, R., Chincarini, G. L., & Haynes, M. P. 1981, ApJ, 247, 383

Griffiths, R. E. et al. 1994, ApJ, 435, L19

Gunn, J. E., & Gott, J. R. 1972, ApJ, 176, 1

Harris, W. E. 1981, ApJ, 251, 497

Henry, J. P., & Lavery, R. J. 1987, ApJ, 323, 473

Hockney, R. W., & Eastwood, J. W. 1981, Computer Simulation Using Particles (New York: McGraw-Hill)

Huang, S. 1995, Ph.D thesis, University of Toronto.

Kaiser, N. 1984, ApJ, 284, L9

Kennicutt, R. C. 1983, AJ, 88, 483

Kent, S. M. 1981, ApJ, 245, 805

Larson, R. B, Tinsley, B. M., & Caldwell, C. N. 1980, ApJ, 237, 692

Lavery, R. K., & Henry, J. P. 1986, ApJ, 304, L5

MacLaren, I., Ellis, R. S., & Couch, W. J. 1988, M.N.R.A.S., 230, 249

Martel, H. 1991a, ApJ, 366, 353

Martel, H. 1991b, ApJ, 377, 7

Martel, H., & Shapiro, P. R. 1997, in preparation.

Martel, H., Shapiro, P. R., & Weinberg, S. 1997, in preparation.

Melnick, J. & Sargent, W. L. W. 1977, ApJ, 215, 401

Mihos, J. C., & Hernquist, L. 1994a, ApJ, 425, L13

Mihos, J. C., & Hernquist, L. 1994b, ApJ, 431, L9

Mobasher, B., Rowan-Robinson, M., Georgakakis, A., & Eaton, N. 1996, M.N.R.A.S., 282, L7

Moore, B., Katz, N., Lake, G., Dressler, A., & Oemler, A. 1996, Nature, 379, 613

Negroponte, J., & White, S. D. M. 1983, M.N.R.A.S., 205, 1009

Noguchi, M. 1988, A&A, 203, 259

Oemler, A. 1992, in Clusters and Superclusters of Galaxies, ed. A. C. Fabian (Dordrecht:Kluwer), p. 29

Ostriker, J. P. 1993, Ann.Rev.A.A., 31, 689

Ostriker, J. P., & Steinhardt, P. J. 1995, Nature, 377, 600

Peebles, P. J. E. 1980, The Large Scale Structure of The Universe (Princeton: Princeton University Press)

Peebles, P. J. E. 1993, Principles of Physical Cosmology (Princeton:Princeton University Press)

Postman, M., & Geller, M. J. 1984, ApJ, 281, 95

Quinn, P. J., & Goodman, J. 1986, ApJ, 309, 472

Quinn, P. J., Hernquist, L., & Fullagar, D. P. 1993, ApJ, 403, 74

Ross, N. 1981, A&A, 95, 349

Sandage A. 1983, in Internal Kinematics and Dynamics of Galaxies, ed. E. Athanassoula (Dordrecht:Reidel), p. 55

Shandarin, S. F. 1980, Astrofizika, 16, 769

Smoot, G. F. et al. 1992, ApJ, 396, L1

Soucail, G., Mellier, Y., Fort, B., & Cailloux, M. 1988, A&A, 73, 471

Spitzer, L., & Baade, W. 1951, ApJ, 113, 413

Toomre, A., & Toomre, J. 1972, ApJ, 178, 623

Toomre, A. 1977, in Evolution of Galaxies and Stellar Populations, eds. B. M. Tinsley and R. B. Larson (New Haven: Yale University Observatory), p. 401

Tóth, G., & Ostriker, J. P. 1992, ApJ, 389, 5

White, S. D. M. 1978, M.N.R.A.S., 184, 185

White, S. D. M. 1979, M.N.R.A.S., 189, 831

Withmore, B. C., Gilmore, D. M., & Jones, C. 1993, ApJ, 407, 489

This preprint was prepared with the AAS LATEX macros v4.0.

Table 1. MORPHOLOGICAL TYPES AT z = 0.

Run	Ellipticals	S0's	Spirals
EdS1	14.5	38.5	47.0
EdS2	14.7	38.7	46.6
EdS3	14.6	38.6	46.8
EdS4	14.8	38.6	46.6
EdS5	14.8	38.7	46.5
O1	13.3	35.9	50.9
O2	13.4	35.6	51.0
O3	13.3	35.0	51.7
O4	13.4	35.7	50.9
O_5	13.1	35.1	51.8
L1	14.4	37.8	47.8
L2	14.7	38.0	47.3
L3	14.3	37.7	48.0
L4	14.3	37.8	47.9
L5	14.6	38.1	47.3

Table 2. TRANSFER OF LOCATION FOR ELLIPTICAL GALAXIES FROM z=3 TO z=0

Run	$\mathrm{L} \to \mathrm{L}$	$\mathrm{L} \to \mathrm{H}$	$\mathrm{H} \to \mathrm{L}$	$\mathrm{H} \to \mathrm{H}$
EdS1	1823	924	785	2440
EdS2	1758	976	820	2434
EdS3	1704	1048	840	2355
EdS4	1780	1079	845	2467
EdS5	1769	1076	817	2517
O1	1686	754	552	2412
O2	1689	745	600	2391
O3	1634	718	623	2423
O4	1675	759	630	2446
O_5	1618	764	640	2217
L1	1834	945	762	2441
L2	1826	995	752	2534
L3	1772	929	781	2514
L4	1790	947	759	2426
L5	1774	1028	774	2502

Table 3. TRANSFER OF LOCATION FOR ALL GALAXIES IN LOW DENSITY REGIONS, FROM $z=3~{\rm TO}~z=0$

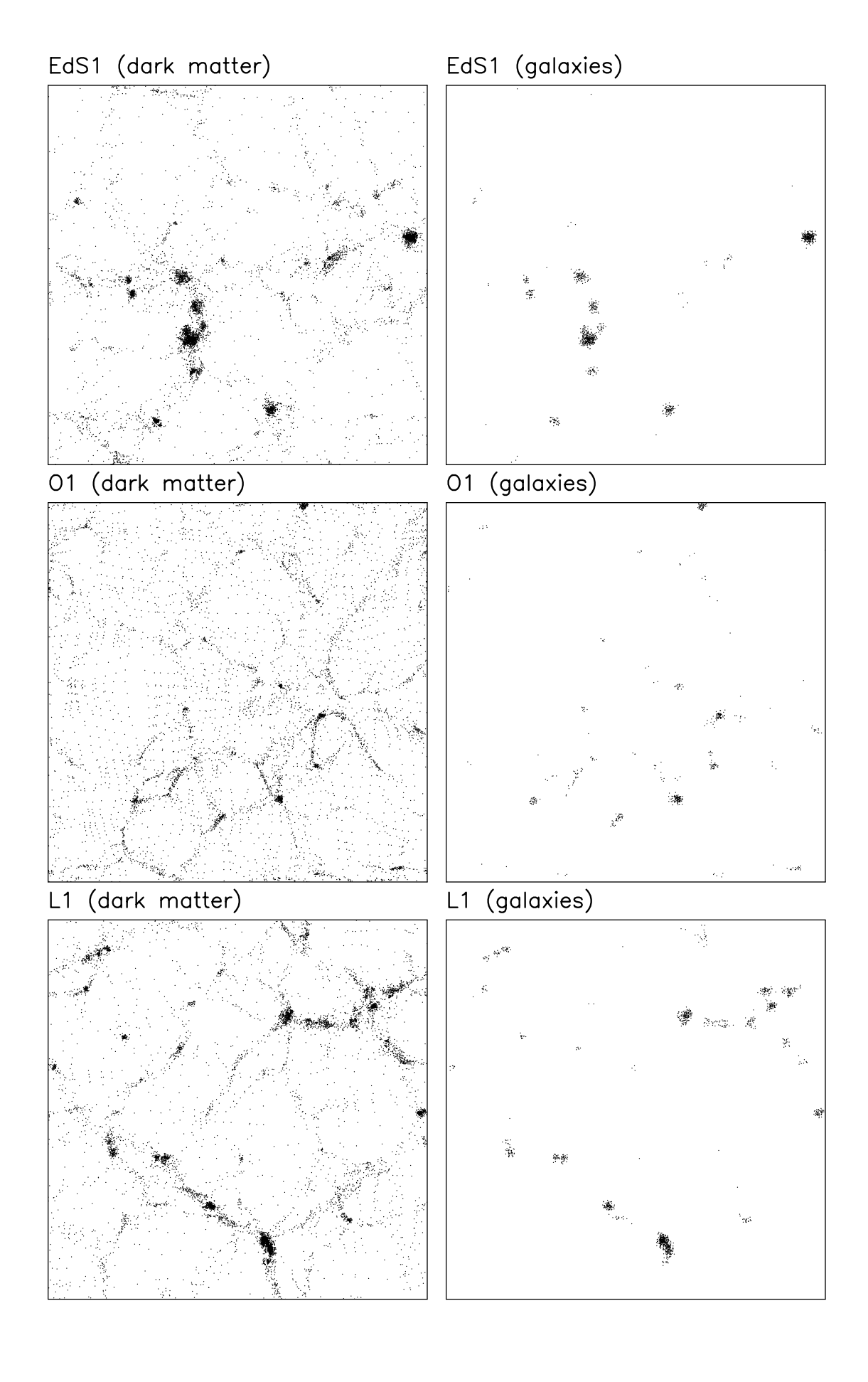
D		$VL \to L$			$\mathrm{VL} \to \mathrm{H}$	
Run	Spirals	$\mathrm{S0's}$	Ellipticals	Spirals	$\mathrm{S0's}$	Ellipticals
EdS1	7813 (53.9)	4863 (33.5)	1823 (12.6)	2576 (42.5)	2565 (42.3)	924 (15.2)
EdS2	7596 (52.9)	4994 (34.8)	1758 (12.3)	2518 (41.4)	2584 (42.5)	976 (16.1)
EdS3	7487 (53.2)	4879 (34.7)	1704 (12.1)	2692 (42.6)	2586 (40.9)	1048 (16.6)
EdS4	7671 (53.0)	5010 (34.6)	$1760 \ (12.3)$	1686 (42.2)	2603 (40.9)	1079 (16.9)
EdS5	7699 (53.0)	5067 (34.9)	1769 (12.2)	2699 (41.4)	2743 (42.1)	$1076 \ (16.5)$
O1	8963 (58.6)	4654 (30.4)	1686 (11.0)	2322 (45.7)	2000 (39.4)	754 (14.9)
O2	9018 (59.4)	4480 (29.5)	1689 (11.1)	2437 (46.4)	2072 (39.4)	746 (14.2)
O3	9101 (60.0)	4429 (29.2)	$1634\ (10.8)$	$2433 \ (47.8)$	1948 (38.1)	718 (14.1)
O4	9057 (58.9)	4655 (30.3)	1675 (10.9)	$2423 \ (46.4)$	2035 (39.0)	760 (14.6)
O_5	8803 (59.1)	4473 (30.0)	1618 (10.9)	$2421 \ (46.8)$	1987 (38.4)	764 (14.8)
L1	8055 (54.7)	4842 (32.9)	1834 (12.4)	2614 (42.9)	2528 (41.5)	945 (15.5)
L2	7956 (54.2)	4901 (33.4)	1826 (12.4)	2586 (42.6)	2493 (41.0)	995 (16.4)
L3	8139 (55.1)	4906 (33.4)	1723 (11.7)	2589 (43.3)	2462 (41.2)	929 (15.5)
L4	8083 (54.8)	4872 (33.0)	1790 (12.1)	2584 (43.4)	$2424 \ (40.7)$	947 (15.9)
L5	8136 (55.2)	4830 (32.8)	$1774\ (12.0)$	2595 (42.5)	2487 (40.7)	$1028\ (16.8)$

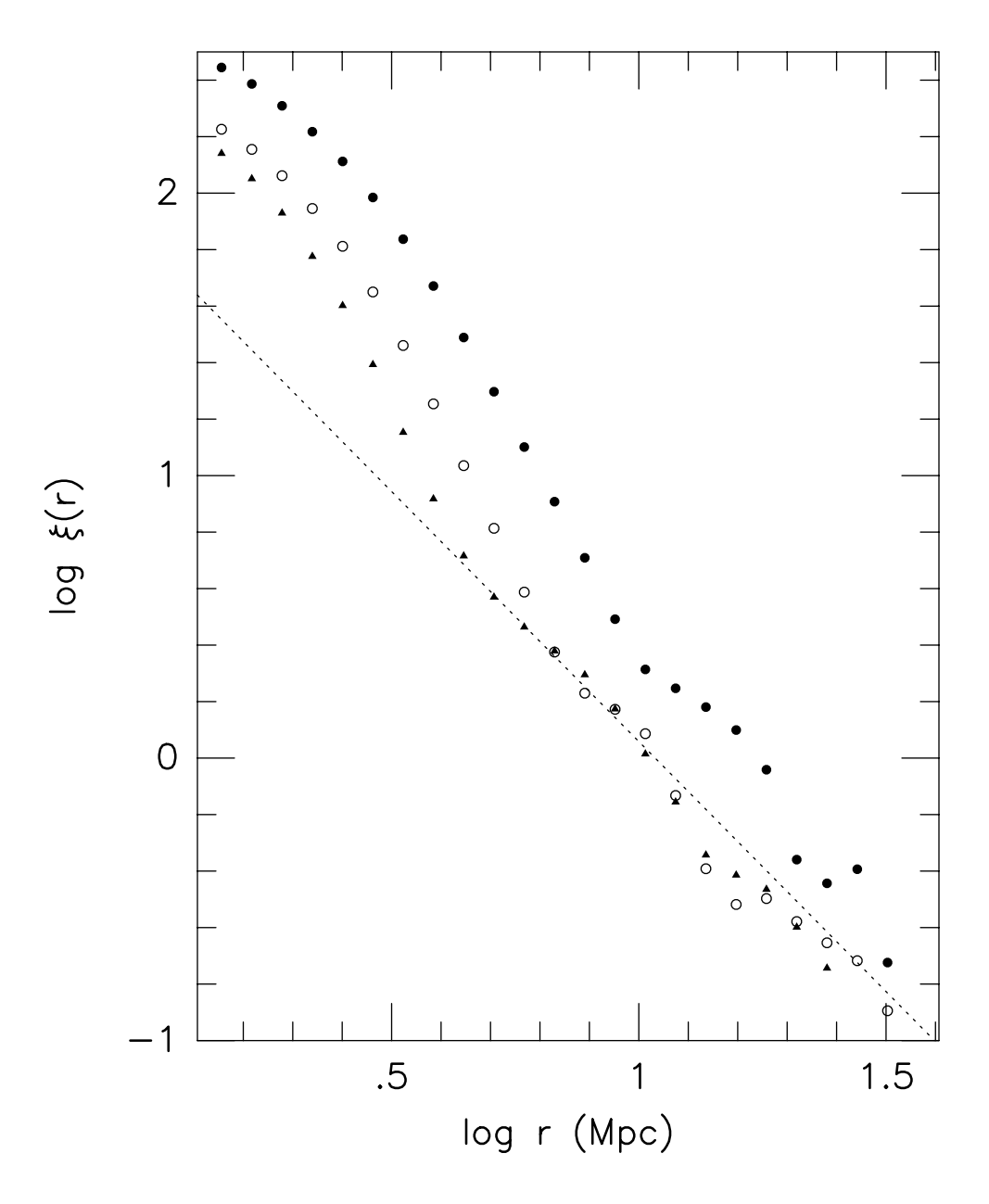
Table 4. TRANSFER OF LOCATION FOR ALL GALAXIES IN VERY LOW DENSITY REGIONS, FROM $z=3~{\rm TO}~z=0$

Run	$\mathrm{VL} \to \mathrm{L}$		$\mathrm{VL} \to \mathrm{H}$			
ıtun	Spirals	S0's	Ellipticals	Spirals	$\mathrm{S0's}$	Ellipticals
EdS1	1124 (61.1)	499 (27.1)	217 (11.8)	104 (48.1)	82 (38.0)	30 (13.9)
EdS2	1076 (60.2)	489 (27.4)	$221\ (12.4)$	113 (44.1)	107 (41.8)	36 (14.1)
EdS3	1018 (58.6)	514 (29.6)	205 (11.8)	129(42.7)	126 (41.7)	47 (15.6)
EdS4	1066 (58.3)	562 (30.7)	202 (11.0)	99(39.3)	101 (40.1)	52(20.6)
EdS5	1133 (61.7)	529 (28.8)	174 (9.5)	106 (39.4)	122 (45.4)	$41\ (15.2)$
O1	1443 (71.2)	391 (19.3)	193 (9.5)	2 (20.0)	4 (40.0)	4 (40.0)
O2	$1491\ (73.1)$	367 (18.0)	183 (9.0)	2(66.7)	1(33.3)	0(0.0)
O3	1429 (70.7)	367 (18.2)	225 (11.1)	1(25.0)	2(50.0)	1(25.0)
O4	1474 (71.8)	374 (18.2)	$206\ (10.0)$	5 (83.3)	1(16.7)	0(0.0)
O_5	1435 (72.0)	373 (18.7)	184 (9.2)	9(64.3)	5(35.7)	0(0.0)
L1	1214 (64.3)	459 (24.3)	215 (11.4)	91 (47.2)	68 (35.2)	34 (17.6)
L2	1246 (64.5)	478 (24.8)	207(10.7)	71 (49.3)	49(34.0)	24 (16.7)
L3	$1238 \ (65.3)$	477(25.2)	180 (9.5)	72 (40.2)	85 (47.5)	$22\ (12.3)$
L4	$1251 \ (65.2)$	470(24.5)	198 (10.3)	71 (47.0)	50(33.1)	30 (19.9)
L5	1272 (65.5)	455 (23.4)	$215\ (10.3)$	62 (43.4)	63(44.1)	18 (12.6)
EdS1*	1119 (62.1)	489 (27.2)	193 (10.7)	105 (41.2)	108 (42.4)	42 (16.5)

Figure Captions

- Fig. 1.— (a) x-y projection of the final positions of the dark matter particles for the run EdS1, with $\Omega_0 = 1$, $\lambda_0 = 0$. (b) x-y projection of the final positions of the galaxies for the run EdS1. (c) and (d): same as (a) and (b) for the run O1, with $\Omega_0 = 0.2$, $\lambda_0 = 0$. (e) and (f): same as (a) and (b) for the run L1, with $\Omega_0 = 0.2$, $\lambda_0 = 0.8$. On all panels, only 1/32 of the computational volume is plotted.
- Fig. 2.— Galaxy 2-point correlation function versus separation, for the Einstein-de Sitter model (filled circles) and the open model (triangles), both at z = 0, and for the Einstein-de Sitter model at z = 0.7 (open circles). The dashed line indicates the observed correlation function.
- Fig. 3.— Population distributions of the various morphological types, vs galaxy number density. Solid curves show the inferred relation, based on the observed morphological type-surface number density of Dressler (1980). Symbols show the numerically generated distributions for all 5 calculations with $\Omega_0 = 1$, $\lambda_0 = 0$ combined. Error bars show the range of values amongst the various calculations. Crosses: Spiral galaxies; Filled circles: S0 galaxies; Open circles: Elliptical galaxies; The number density ρ is in galaxies/Mpc³.
- Fig. 4.— Galaxy distributions at various redshifts for the run EdS1. Only 1/8 of the computational volume is plotted.
- Fig. 5.— L \rightarrow H and H \rightarrow L counts versus probability p for the probabilistic model. Top panel: Einsteinde Sitter model; middle panel: open model; bottom panel: cosmological constant model.
- Fig. 6.— Time-evolution of the number density of galaxies around each elliptical galaxies described in the text as a "VL \rightarrow H elliptical," plotted as a function of redshift z, for all runs for which there are such galaxies. The number density n is in units of Mpc³.
- Fig. 7.— Location of the galaxies at z=3 for the EdS1 and EdS1* runs in computational units. (a) x-coordinate of galaxies in the EdS1* run versus same coordinates in the EdS1 run. (b) Histogram of the distance between each galaxy in the EdS1 run and its counterpart in the EdS1* run. Each bin has a width of 800 kpc in physical units.





fraction of population

